JOURNAL OF PROPULSION AND POWER
Vol. 11, No. 3, May–June 1995

Flows in a Curved Combustor Inlet with and Without a Guide Vane

Tong-Miin Liou* and Chin-Chun Liao†
National Tsing Hua University, Hsin-Chu, Taiwan 30043, Republic of China

Laser Doppler velocimetry measurements of the longitudinal, radial, and spanwise velocity components are presented for the three-dimensional flowfield in a 60-deg curved combustor inlet duct with and without a guide vane. The Reynolds number based on the bulk mean velocity and hydraulic diameter was 2.53×10^4. Quantities such as mean-velocity vectors, wall static pressure, size of the reversed flow region, number of secondary vortex pairs, streamwise mean vorticity, turbulence intensity contours, anisotropy, turbulent kinetic energy, and structure parameters were used to characterize the flow. Comparisons between the flow characteristics within the curved duct with and without a guide vane were also made. It was found that the presence of a guide vane partially suppresses formation of the region of flow reversal, provides a more uniform velocity distribution across the inner passage of the curved duct, and enhances a stronger secondary flow vortex in the cross-stream section.

Nomenclature

a, b	=	cross-section radius, and spanwise dimension, mm
C_p	=	pressure coefficient, $\equiv(P - P_{ref})/(\frac{1}{2}\rho U_{ref}^2)$
D_h	=	hydraulic diameter, mm
k	=	turbulent kinetic energy, $\equiv 1/2(\overline{u^2} + \overline{v^2} + \overline{w^2})$, m²/s²
P	=	wall static pressure, Pa
P_{ref}	=	reference value of P ($X_h^* = -5$, $R_h^* = 0.5$), Pa
Re	=	Reynolds number, $\equiv D_h U_{ref}/\nu$
R_h, Z_h	=	radial, spanwise coordinate, mm
R_h^*	=	normalized radial coordinate (measurement plane parallel to longitudinal direction), $R_h^* = R_h/(R_o - R_i)/2 = R_h/a/2$
R_h^{**}	=	normalized radial coordinate (measurement plane parallel to dump plane), $R_h^{**} = R_h/(R_o - R_i)/2\cos(30\text{ deg})$
R_i, R_o, R_m	=	curved duct inner, outer, and mean radius ($R_i = 23.5$, $R_o = 70.5$, $R_m = 47$), mm
U, V, W	=	longitudinal, radial, and spanwise mean velocity, m/s
U_{ref}	=	longitudinal bulk mean velocity, 9.9 m/s
u, v, w	=	longitudinal, radial, and spanwise fluctuating velocity, m/s
$\overline{v^2} - \overline{w^2}$	=	difference of normal stresses, m²/s²
X_h, θ_h	=	longitudinal coordinate, mm, deg
X_h^*	=	normalized longitudinal coordinate (measurement plane parallel to longitudinal direction), $X_h^* = X_h/D_h$
X_h^{**}	=	normalized longitudinal coordinate (measurement plane parallel to dump plane), $X_h^* = X_h/D_h$
Z_h^*	=	normalized spanwise coordinate, $Z_h^* = Z_h/(b/2)$
ν	=	kinematic viscosity, m²/s
ρ	=	air density, kg/m³
Ω	=	streamwise vorticity, s⁻¹

Subscript

max	=	maximum value within individual cross-sectional plane

Received Jan. 14, 1994; revision received Aug. 26, 1994; accepted for publication Sept. 1, 1994.

*Professor, Power Mechanical Engineering Department.
†Graduate Student, Power Mechanical Engineering Department.

Introduction

FLUID flows in curved ducts are widely observed in pipe systems, arterial systems, and aircraft intakes. The curvature of a curved duct induces secondary flows and complex turbulent characteristics. The secondary flow, driven mainly by the imbalance between the centrifugal force and the radial pressure gradient, causes redistribution of the streamwise main flow, a larger pressure drop, and enhanced rates of heat, mass, and momentum transfer. A full account of the generation of the secondary flow can be found in Ward-Smith.[1] The characteristic of the flowfield in the curved inlet duct of a side-dump combustor has a direct effect on the performance of the succeeding combustor. A clear understanding of the evolution of the flowfields and the effects of the secondary flow in the curved ducts is therefore important in engineering design.

In early research, the secondary flow was only qualitatively understood by means of flow visualization techniques. Eustice[2] demonstrated the existence of a secondary flow by injecting ink into water flowing through a coiled pipe. In 1974, Austin and Seader[3] measured the longitudinal velocity profiles in coiled circular pipes by means of a hot-film anemometry system. Recently, the development of the laser Doppler velocimetry (LDV) technique has given more accurate and detailed velocity measurements. Measurements of the laminar and turbulent water flow in curved ducts have been reported, e.g., by Agrawal et al.,[4] Humphrey et al.,[5,6] and Taylor et al.[7] They found that the boundary-layer thickness at bend entry influenced the flow development and strength of the secondary flow. As for the airflow, Holt et al.[8] and Liou et al.[9,10] studied the developing turbulent flow in 90-deg curved square ducts. Liou et al.[9,10] investigated the effects of the Reynolds number and the aspect ratio (b/a) on the flowfield in a 90-deg curved square duct, and demonstrated that as the aspect ratio increased, the strength of the main secondary flow decreased. Computational analysis of the turbulent flow in curved square ducts has been conducted by Pratap and Spalding,[11] Iacovides et al.,[12] and Govindan et al.[13] Pratap and Spalding[11] solved the three-dimensional time-averaged Navier-Stokes equations, incorporating a two-equation turbulence model to study the flow in a curved rectangular duct. Iacovides et al.[12] studied the turbulent flow around a square-

sectioned U-bend by a three-dimensional finite volume solver employing an algebraic second-moment (ASM) turbulence model, and compared the results with their own experimental data obtained by hot-wire anemometry. They suggested that the secondary flow broke down into multiple vortices on either side of the midplane. Govindan et al.[13] derived generalized primary/secondary flow equations and computed solutions for flow in 90-deg bends, which agreed well with the experimental data compiled by Taylor et al.[7] Most of the preceding investigations were restricted to the topic of curved ducts with circular and rectangular cross sections. As for the curved ducts with other sections, Dong et al.[14] has even conducted study on the fully developed laminar flow in the curved duct with an elliptic cross section, revealing that in every computation there is only one pair of secondary vortices. In addition, Ghia et al.,[15] by solving the Navier-Stokes equations, have investigated the fully developed flows in curved ducts of rectangular and polar cross sections. Their results showed that the phenomenon of Dean's instability was observed in ducts of square cross section, but not in polar cross-section ducts. Some review articles on the flow and heat transfer in curved pipes have been presented by Berger et al.,[16] Itō,[17] and Shah et al.[18]

There are relatively few works on curved ducts installed with guide vanes. For engineering use, most previous experiments were carried out to provide information on pressure losses in vaned elbows of rectangular and circular cross sections.[19,20] A more recent study[21] was performed numerically for laminar and turbulent flows in a two-dimensional bend with or without a guide vane. The turbulence model adopted was the k-ε model, and the TEACH-T computer program was used. However, because the realistic flow in a curved duct is three dimensional and highly anisotropic, there is still a need to perform quantitative and three-dimensional measurements of detailed mean velocity field and turbulence parameters to furnish useful data for this class of flow. The brief survey presented above reveals the lack of three-dimensional flow measurements in curved ducts with and without installing guide vanes. The aim of this article is therefore to investigate the three-dimensional developing turbulent flow in the 60-deg rectangular inlet duct with/without a guide vane located upstream of a side-dump combustor using LDV for three velocity components (longitudinal, radial, and spanwise) and, accordingly, to demonstrate the effect of adding a single guide vane. LDV was chosen for the present work since the flow reversal and large turbulence fluctuations were expected in part of the curved duct. Another purpose of this work is to provide researchers with a useful reference to develop both turbulence and numerical models for predicting the flowfields in such a curved inlet duct. In addition, flow measurements near the dump plane of a side-dump combustor provide a more realistic inlet boundary condition for combustor flow modeling.

Experimental Apparatus and Conditions

Experimental System

The flow system and LDV experimental setup in the present work is similar to that described in Liou and Wu.[22] Air was drawn into the curved side inlet through a settling chamber and a 10:1 bell-mouth-like contraction by a blower at the downstream end. The settling chamber contained a flow straightener and six screens. The air then flowed into the curved inlet ducts, the combustion chamber, a flow straightener, a flowmeter, a bellows, and was exhausted by the blower. A dual beam LDV system was set up in a forward or off-axis scattering configuration. A 300-mW helium-neon laser with a 632.8-nm (red) line provided the coherent light source. The approximate probe-volume dimensions were 0.57 mm in length and 0.18 mm in diam. The LDV system mentioned above was utilized to measure the longitudinal and radial velocity components from the side wall of the curved inlet duct. The spanwise velocity component was measured from the outer wall of the curved duct, using a one-component fiber-optic probe LDV system whose light source was a linearly polarized 300-mW argon ion laser (514.5-nm wavelength), and whose probe-volume dimensions were approximately 0.14 × 2.4 mm. The detailed optical arrangement of this portable backscattering LDV system was described in Tsai and Liou[23] for a study of flow induced by nonuniform lateral injection. The entire LDV system was mounted on a milling machine with four vibration isolation mounts, allowing the probe volume to be positioned with 0.01-mm resolution. The light scattered from salt particles with a nominal 0.8 μm was collected into a photomultiplier and subsequently downmixed to the appropriate frequency shift of 2–5 MHz. A counter processor with 1-ns resolution was used to process the Doppler signal. The Doppler signal was monitored on an oscilloscope, and the digital output of the counter processor was fed directly to a microcomputer for storage and analysis.

Curved Duct Model and Test Conditions

The configuration of the curved duct model, coordinate system, and dimensions for the one-vane case are shown in Fig. 1. Geometry of the curved inlet duct without a guide vane is the same as that shown in Fig. 1 except for the lack of the guide vane. The inlet duct, made of 5-mm Plexiglas®, consists of an upstream tangent, a 60-deg bend of mean radius R_m 47 mm, and a downstream tangent. The upstream tangent is a straight rectangular duct with a length of 370 mm. The inner and outer radii of the 60-deg bend are 23.5 and 70.5 mm, respectively. The downstream tangent consists of an outer radius wall of 61.8 mm and an inner radius wall of 34.7 mm length. The internal dimensions of the cross section are 47 × 35 mm ($a \times b$), the corresponding hydraulic diameter D_h is 40 mm, and the radius ratio R_m/D_h is 1.2. The shape of the guide vane is a circular-arc, from the bend entry plane to the bend-exit plane. In addition, the guide vane has a straight extension of $0.25D_h$ at the leading edge and at the trailing edge that extends to the dump plane. With a thickness of $0.025D_h$, the guide vane is positioned in the middle of the duct. The two rectangular inlet ducts intersect the combustor at an inlet angle of 60 deg. The centerlines of both inlet ducts intersect the combustor at the same axial station and are located circumferentially at 180 deg to each other. The in-

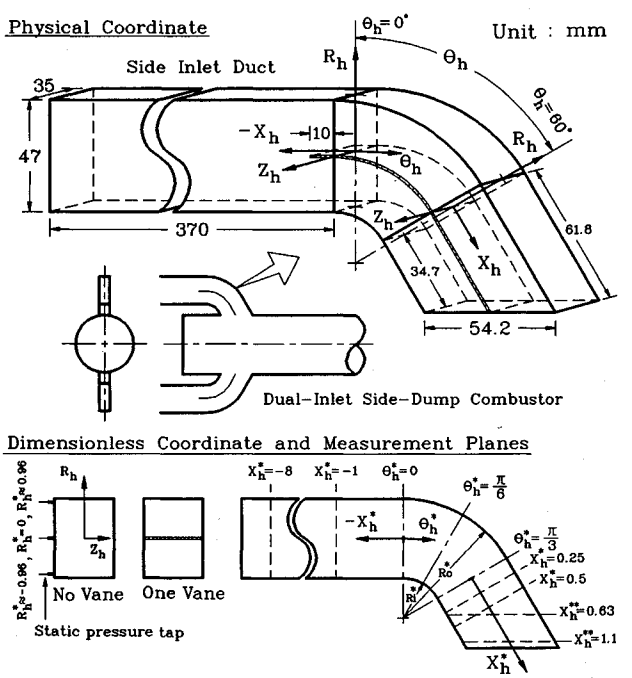

Fig. 1 Sketch of configuration, dimensions, coordinate system, and measurement planes of curved inlet duct.

ternal dimensions of the dump plane are 35 × 54.2 mm. There are three coordinate systems in the present work, each for a given zone: two separate Cartesian systems, one each for the straight ducts (negative X_h^* for the upstream tangent and positive X_h^* for the downstream tangent) and a cylindrical system for the bend.

The longitudinal and radial velocity measurements for the one-vane and no-vane cases were made at six longitudinal stations: $\theta_h = 0$ deg, $\theta_h = 30$ deg, $\theta_h = 60$ deg, $X_h^* = 0.25$, $X_h^{**} = 0.63$, and $X_h^{**} = 1.1$. The measurements for the spanwise velocity were made at three longitudinal stations: $\theta_h = 30$ deg, $\theta_h = 60$ deg, and $X_h^* = 0.25$. There were five spanwise stations, $Z_h^* = 0.89$, 0.69, 0.46, 0.23, and 0, for the measurements of all three components. Note that the $X_h^{**} = 0.63$ and $X_h^{**} = 1.1$ stations were located at 0.5 and $0.1D_h$, respectively, above the combustor inlet port owing to the limitation of the inlet flange, and were chosen to be parallel with the combustor side walls instead of perpendicular to the duct walls to provide appropriate inlet boundary conditions for combustor modeling. The measuring positions were chosen to give a clear pattern of the flow field. The bulk mean velocity, 9.9 m/s, was used as a reference (U_{ref}) to normalize the results. The Reynolds number based on the bulk mean velocity and hydraulic diameter was 2.53 × 10^4, indicating the flow to be turbulent. The corresponding Dean number $[Re(D_h/2R_m)^{0.5}]$ was 1.65 × 10^4. The guide vane divided the curved duct into two segments defined as the outer passage and inner passage, as shown in Fig. 1. The corresponding hydraulic diameter and Reynolds number for these two segments were 28 mm and 1.76 × 10^4, respectively. The mean radius, radius ratio, and Dean number for the outer passage were 59 mm, 2.1, and 8.54 × 10^3, respectively, and 35 mm, 1.3, and 1.11 × 10^4, respectively, for the inner passage.

Results and Discussion

Data Accuracy

The presented mean velocity and turbulence intensity were calculated from the probability distribution function of the measurements. Typically, 2000–4000 realizations were averaged at each measuring location. The corresponding statistical errors in the mean velocity and turbulence intensity were less than 1.8 and 3.1%, respectively, for a 95% confidence level. More detailed uncertainty analyses such as velocity gradient broadening, data repeatability, velocity bias correction, etc., were included in the work of Liou and Kao[24] and Liou et al.[25] Verification of the spanwise symmetry of the mean velocity and turbulence intensity was performed for various streamwise stations, and the deviations of the mean velocity and turbulence intensity for three components were found to be within 0.028 and $0.015U_{ref}$, respectively. Accordingly, in each of the measuring planes data were collected only in the symmetrical half. To check the conservation of the mass flow rate, the mean longitudinal velocities were also integrated over each cross section. The results showed that the continuity errors of all the cross-sectional planes were within 3.8 and 3.4% for the no-vane and one-vane case, respectively.

Upstream Tangent

Measurements of the longitudinal mean velocity and turbulence intensity at $X_h^* = -8$ and $X_h^* = -1$ in the upstream tangent were made; only the results at $X_h^* = -1$ are shown in Fig. 2 for the one-vane case. At $X_h^* = -8$, the core fluid occupies, except near the duct wall, almost the entire cross-stream plane (about 84%), indicating an essentially uniform longitudinal mean velocity profile as a result of the acceleration of the 10:1 bell-mouth-like contraction. As the flow proceeds to $X_h^* = -1$, the region of core fluid is narrowed to 53% of the cross-stream plane, which suggests that the fluid flowing into the bend entry plane is a hydrodynamically developing flow. The edges of the boundary layers (defined at 0.95 of the maximum longitudinal velocity at each longitudinal station) at $X_h^* = -8$ and $X_h^* = -1$ are located at a distance less than 0.085 and $0.17D_h$, respectively, from the walls. The latter value is comparable to that reported by Taylor et al.[7] who measured the boundary-layer thickness of $0.15D_h$ at the bend inlet ($X_h^* = -0.25$) in a 90-deg curved duct without installing guide vanes and with a Reynolds number of 4 × 10^4. The thickness of the boundary layer at the bend entry plane is important to the evolution and magnitude of the secondary flow.[7] The mean velocity profile in the boundary layer is near the one-seventh-power law profile, and the shape factor is 1.5 at $X_h^* = -1$. These results suggest that the boundary layer at $X_h^* = -1$ is turbulent. The corresponding turbulence intensity at $X_h^* = -8$ is quite low, except near the walls, with a value as high as 2% U_{ref} over about 75% of the cross-stream plane. Figure 2 shows that the turbulence intensity at station $X_h^* = -1$ increases progressively with a region of 20% of the cross-section plane within a value of 2% U_{ref}.

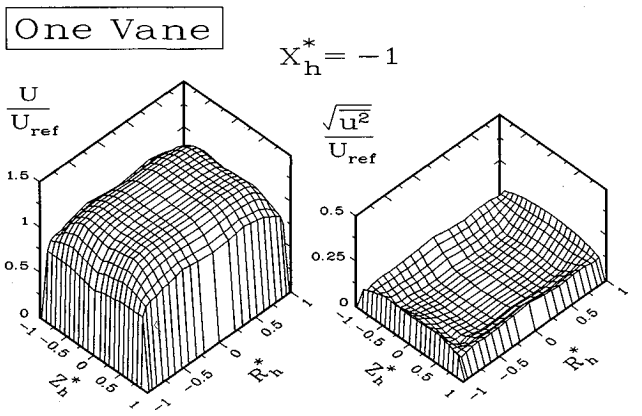

Fig. 2 Distributions of longitudinal mean velocity and turbulence intensity at $X_h^* = -1$.

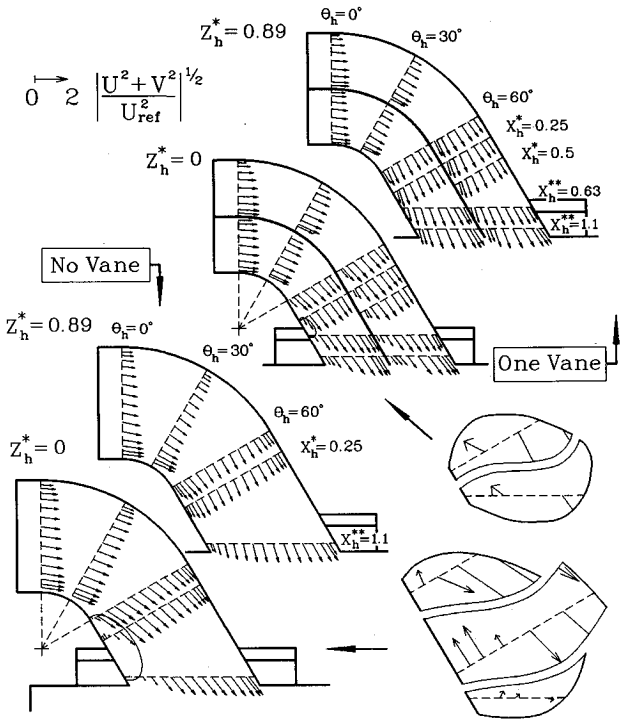

Fig. 3 Streamwise mean flow pattern in terms of velocity vectors at $Z_h^* = 0$ and 0.89 for one-vane and no-vane cases.

Flowfield in Longitudinal Plane Z_h

The streamwise evolution of the longitudinal and radial mean velocity components along $Z_h^* = 0$ and 0.89 planes for

both one-vane and no-vane cases is depicted in Fig. 3 in terms of the resultant vector plots. The flow distortion and the separation adjacent to the inner wall of the inner passage in the downstream tangent are clearly visible. Note that the separated recirculation zone in the one-vane case is smaller than that in the no-vane case. The streamwise mean velocity displays an acceleration near the inner wall and a deceleration near the outer wall for the front part of the duct, but for the latter part of the bend it is reversed. The aforementioned phenomenon results from the influence of the longitudinal pressure gradient and can be seen in most of the curved ducts. Figure 4 shows the wall static pressure vs streamwise distance at various Reynolds numbers for the no-vane case. The radial pressure gradient becomes larger from about $X_h^* = -1.5$, indicating that the bend has little effect on the flow $1.5D_h$ upstream of the bend inlet. Initially, there is a favorable pressure gradient along the inner wall, accompanied by an adverse gradient along the outer wall. These pressure distributions cause the acceleration and deceleration of the fluid observed near the respective walls, and these trends are reversed after $\theta_h = 30$ deg. The largest pressure difference between the outer and inner walls is at $\theta_h = 30$-deg plane. Another observation is that the pressure distributions for different Reynolds numbers have the same tendency except near the latter part of the bend along the inner wall. For the latter part of the bend, the radial pressure difference increases with decreasing Reynolds number.

Figure 5 depicts the distribution of the longitudinal mean velocity and turbulence intensity along the inner walls (at a distance of 1 mm from the inner walls of the no-vane case as well as of the inner and outer passages of the one-vane case) at $Z_h^* = 0$. Along $R_h^* \simeq -0.96$, the longitudinal mean velocity decelerates significantly for the latter part of the bend and becomes negative approximately from $\theta_h \simeq 57$ deg to the exit plane of the curved inlet duct, and from $X_h^* \simeq 0.05$ to $X_h^* \simeq 0.39$ for no-vane and one-vane cases, respectively. The reversed longitudinal mean velocity reaches values as high as $-0.35U_{ref}$ and $-0.1U_{ref}$ for no-vane and one-vane cases, respectively. The steep longitudinal mean velocity gradient associated with the significant flow deceleration leads to high longitudinal turbulence intensities in these regions, with maximum turbulence intensities as high as $0.34U_{ref}$ at $\theta_h \simeq 57$ deg and $0.37U_{ref}$ at $\theta_h = 60$ deg for no-vane and one-vane cases, respectively. As for $R_h^* \simeq 0.06$ of the one-vane case, the longitudinal mean velocity decelerates all the way in the bend until $\theta_h = 60$ deg, with a minimum velocity of $0.12U_{ref}$ and a corresponding turbulence intensity as high as $0.21U_{ref}$, and then accelerates downstream without separation. Figure 6 plots the boundaries of the reversed flow region where the longitudinal component of velocity is negative along the $X_h^* = 0.25$, $Z_h^* = 0$, and $R_h^* \simeq -0.96$ planes. It is interesting to note that the reversed flow first starts at the quarter plane,

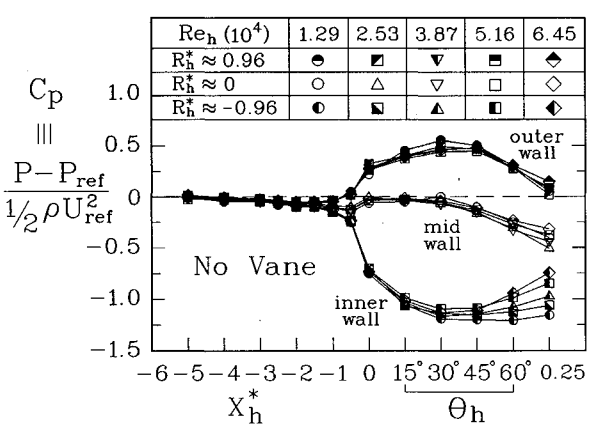

Fig. 4 Wall static pressure vs streamwise distance at various Reynolds numbers for no-vane case.

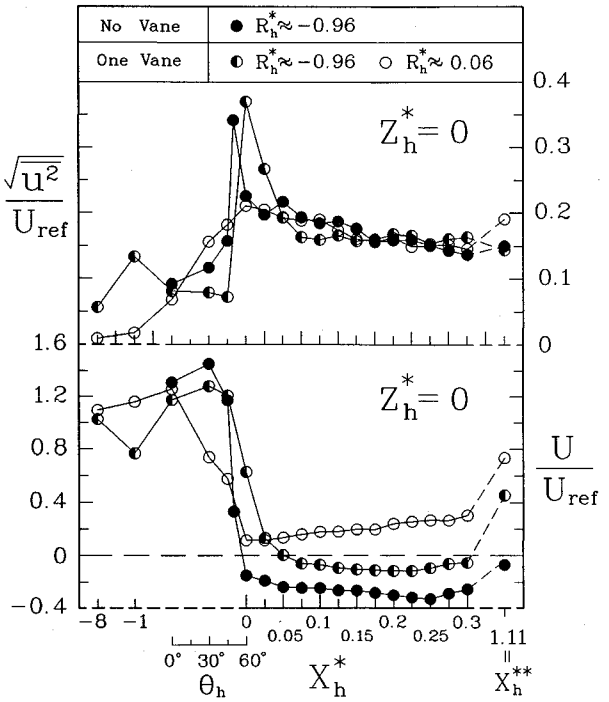

Fig. 5 Longitudinal mean velocity and turbulence intensity distributions along $R_h^* \simeq -0.96$ for no-vane case and $R_h^* \simeq -0.96$ and $R_h^* \simeq 0.06$ for one-vane case in $Z_h^* = 0$ plane.

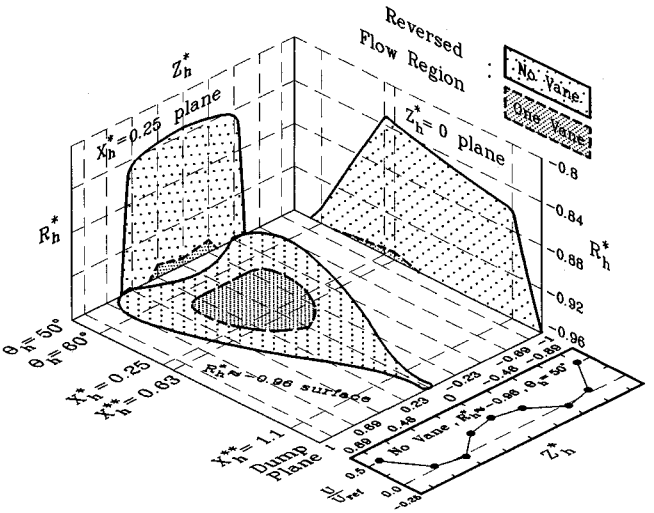

Fig. 6 Boundaries of reversed flow regions for one-vane and no-vane cases.

not at the central plane of the duct for the no-vane case. Therefore, the front of the reversed flow region forms an approximately concave shape (the maximum asymmetry in the reversed flow region is within $0.15U_{ref}$, based on measurements made in both symmetric halves); sequentially, it shrinks quickly as the flow proceeds downstream. This phenomenon can be further supported from the profile of the longitudinal mean velocity at $\theta_h = 50$ deg along the spanwise direction for the no-vane case shown in the lower part of Fig. 6. The negative velocities occur only in the vicinity of $Z_h^* = \pm 0.46$, indicating that the separation occurs at the quarter plane sooner than it does in the central plane. The separation in the one-vane case has a similar shape; however, its size is smaller than that of the no-vane case. The size of the reversed flow region along the inner wall is found to have an area of 0.32 and $0.08D_h^2$ at $R_h^* \simeq -0.96$, and a maximum height of 0.1 and $0.03D_h$ at $X_h^* = 0.25$ for the no-vane and one-vane cases, respectively. By installing a single guide vane in the

curve inlet duct, the size of the separated flow region along the inner wall is narrowed to about 25% of the original size observed for the case without a guide vane.

Spanwise Mean Flow Structure

Very few investigations have been carried out experimentally to identify the significant effect of the secondary flow on the flowfield in a curved duct by measuring both radial and spanwise velocity components. Therefore, a direct measurement of the secondary flow in the curved duct is worthwhile, and the results of the longitudinal mean velocity contours and secondary velocity vectors at $\theta_h = 30$ deg, $\theta_h = 60$ deg, and $X_h^* = 0.25$ for one-vane and no-vane cases are shown in Fig. 7. A pair of counter-rotating vortices (hereafter referred to as the main secondary flow vortices) is generated in the cross section by the imbalance between the centrifugal force and the radial pressure gradient. The secondary flow motion displaces high-speed fluid towards the outer wall along the region containing the central plane, and low-speed fluid towards the inner wall along the side wall. These main secondary flow vortices are narrow and prevail near the side walls. The main secondary vortex center, plotted in Fig. 7 as an open circle, moves progressively towards the inner wall for the no-vane case, and towards the central plane for the one-vane case. It is worth noting that, apart from the main secondary flow vortices, there is a pair of additional secondary flow vortices adjacent to the inner wall at $X_h^* = 0.25$ for the no-vane case. This is because the flow is reversed near the central inner wall, and consequently, the main secondary flow vortices are distorted to accommodate the additional secondary flow vortices. In the one-vane case, the additional vortices are not apparent because of the weaker reversed flow. Due to convective transfer of low-momentum fluid by the side-wall secondary flow from the outer wall to the inner wall and the influences of flow separation, the core flow and maximum longitudinal mean velocity position are displaced progressively from the regions near the inner walls towards the center of the duct as the fluid flows downstream from $\theta_h = 30$ deg to $X_h^* = 0.25$. The positive radial mean velocities at $\theta_h = 60$ deg are greater than those at $\theta_h = 30$ deg and $X_h^* = 0.25$ due to the centrifugal force generated by the curvature and disappear in the downstream tangent. Thus, the radial mean velocity reaches a value as high as 0.68 and $0.43U_{ref}$ for the no-vane and one-vane cases, respectively. It was found that the negative radial velocities, which are restricted to a small region adjacent to the side walls, are far smaller than the positive radial velocities in the region containing the symmetry plane. This result is contrary to the measurements of Taylor et al.[7] and Liou and Liu[9] in a 90-deg square duct, as well as Chang et al.[26] in a square-sectioned U-bend. The difference is due to the smaller curved angle that induces the weaker secondary flow in the present work. The maximum negative

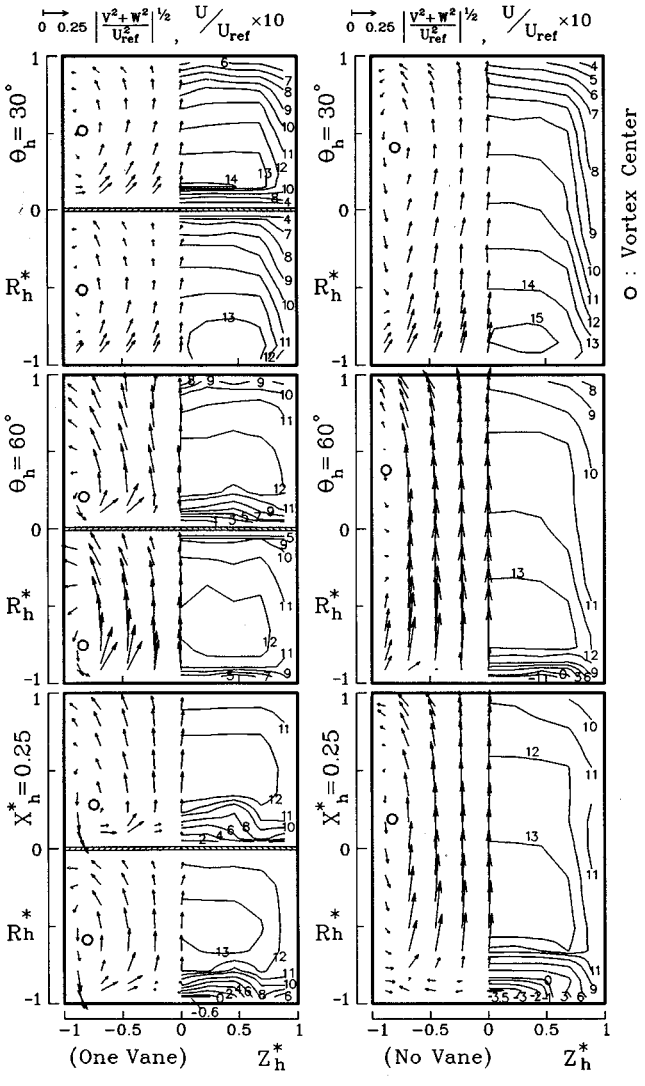

Fig. 7 Secondary mean flow pattern in terms of velocity vectors and longitudinal mean velocity contours at three selected cross-sectional planes for one-vane and no-vane cases.

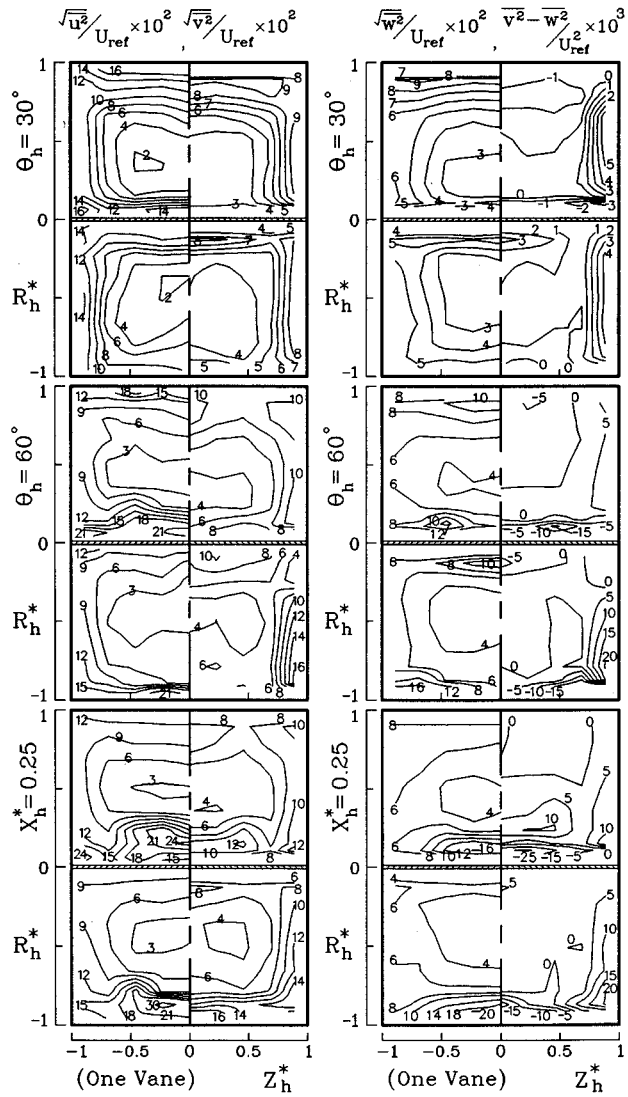

Fig. 8 $\sqrt{\overline{u^2}}$, $\sqrt{\overline{v^2}}$, $\sqrt{\overline{w^2}}$, and $\overline{v^2} - \overline{w^2}$ contours at three selected cross-sectional planes for one-vane case.

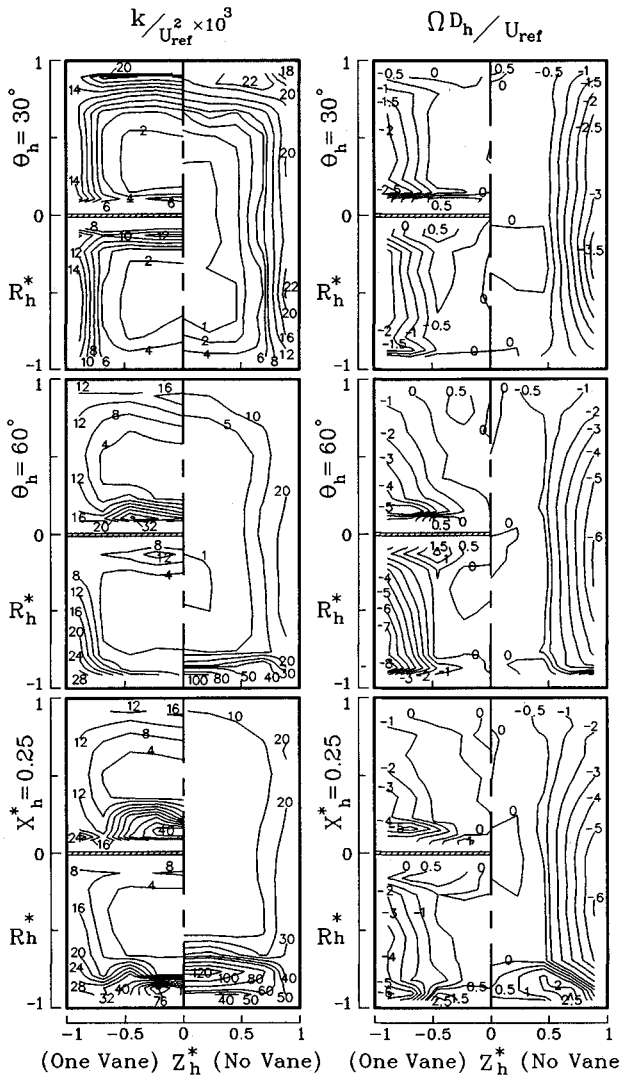

Fig. 9 Turbulent kinetic energy and streamwise mean vorticity contours at three selected cross-sectional planes for one-vane and no-vane cases.

radial velocities found at $X_h^* = 0.25$ are about 0.15 and $0.22U_{ref}$ for the no-vane and one-vane cases, respectively, which is smaller than $0.35U_{ref}$ in Liou and Liu,[9] and $0.4U_{ref}$ in Taylor et al.[7] and Chang et al.[26] The longitudinal mean velocity contours reveal that there are negative values near the inner wall at $X_h^* = 0.25$, indicating the presence of the additional secondary vortices mentioned above. The maximum positive spanwise mean velocities (not shown in Fig. 7) found at $\theta_h = 60$ deg are about 0.12 and $0.18U_{ref}$ for the no-vane and one-vane cases, respectively.

Turbulence Level and Isotropy

The transport of the turbulence energy along the side walls from the outer wall to the inner wall by the motion of secondary flow results in high levels of turbulence intensity and the appearance of shear stresses at the side walls. The contour maps of the longitudinal, radial, and spanwise turbulence intensity components shown in Fig. 8, and the turbulent kinetic energy shown in Fig. 9, illustrate the aforementioned effects. All three turbulence intensity components and the turbulent kinetic energy are higher near the outer wall than near the inner wall in the first part of the bend; this trend is reversed in the latter part of the bend and the downstream tangent. It can also be seen that the maximum turbulence levels

$$\sqrt{\overline{u^2}_{max}},\ \sqrt{\overline{v^2}_{max}},\ \sqrt{\overline{w^2}_{max}},\ \text{and}\ \ k_{max}$$

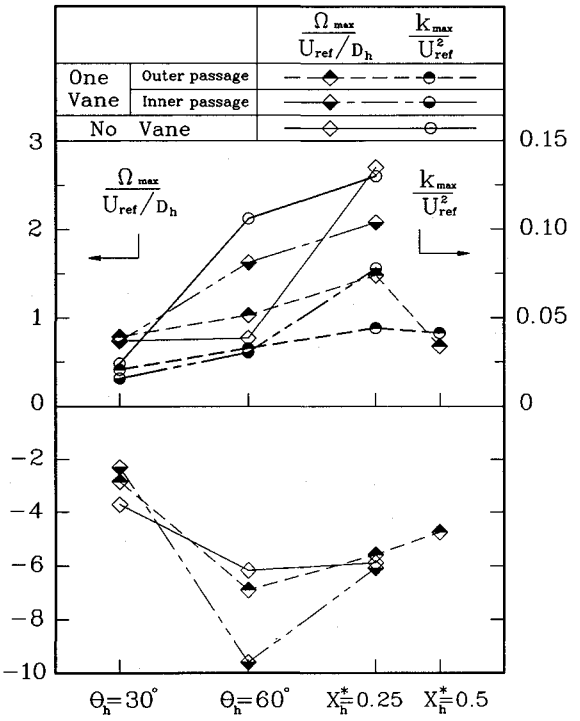

Fig. 10 Variation of maximum Ω and k with streamwise distance.

increase with increasing streamwise distance. Figure 10 provides an example that shows the increase of k_{max} with longitudinal distance. At $X_h^* = 0.25$, the

$$\sqrt{\overline{u^2}_{max}},\ \sqrt{\overline{v^2}_{max}},\ \sqrt{\overline{w^2}_{max}},\ \text{and}\ \ k_{max}$$

are $0.41U_{ref}$, $0.19U_{ref}$, $0.25U_{ref}$, $0.12U_{ref}^2$ for the no-vane case, and $0.34U_{ref}$, $0.16U_{ref}$, $0.2U_{ref}$, $0.08U_{ref}^2$ for the one-vane case.

The interchange of the turbulence energy between the inner and outer wall due to the secondary flow motion, and the redistribution between normal stresses, turbulent diffusion, and dissipation are responsible for the occurrence of the regions with relatively strong anisotropy in the curved duct. For example, at the exit plane of the bend for the no-vane case, the ratio $\overline{u^2}/\overline{v^2}$ is between 3.1–6.23 at the inner wall, and 0.83–2.3 at the outer wall. This observation indicates that the flow at the outer wall is more isotropic than that at the inner wall, and is in agreement with the results of Humphrey et al.,[6] who found $1.6 < \overline{u^2}/\overline{v^2} < 4.6$ at the inner wall and $0.5 < \overline{u^2}/\overline{v^2} < 1.4$ at the outer wall for the turbulent flow in a 90-deg square duct. Figure 11 depicts the distribution of the regions of the relative order of

$$\sqrt{\overline{u^2}},\ \sqrt{\overline{v^2}},\ \text{and}\ \ \sqrt{\overline{w^2}}$$

as well as the contour map of the structural parameters of $\overline{u^2}/k$, $\overline{v^2}/k$, and $\overline{w^2}/k$ at the $X_h^* = 0.25$ station for the one-vane case. Note the region where

$$\sqrt{\overline{u^2}} > \sqrt{\overline{v^2}} > \sqrt{\overline{w^2}}$$

occupies about 30% area of the cross-sectional plane. The $\overline{u^2}/k$, $\overline{v^2}/k$, and $\overline{w^2}/k$ are typically 0.97, 0.49, and 0.55, respectively, for the plane shear layer.[27] These values also exist at the shear layer near the separated region in the present work. From the lower plots of Fig. 11, the highest percentages of the data of $\overline{u^2}/k$, $\overline{v^2}/k$, and $\overline{w^2}/k$ lie around values of 0.81, 0.72, and 0.46, respectively, at the $X_h^* = 0.25$ station. The difference between the structural parameters in the present work and those of Launder et al.[27] is attributable to the influence of the curvature and should provide useful information for

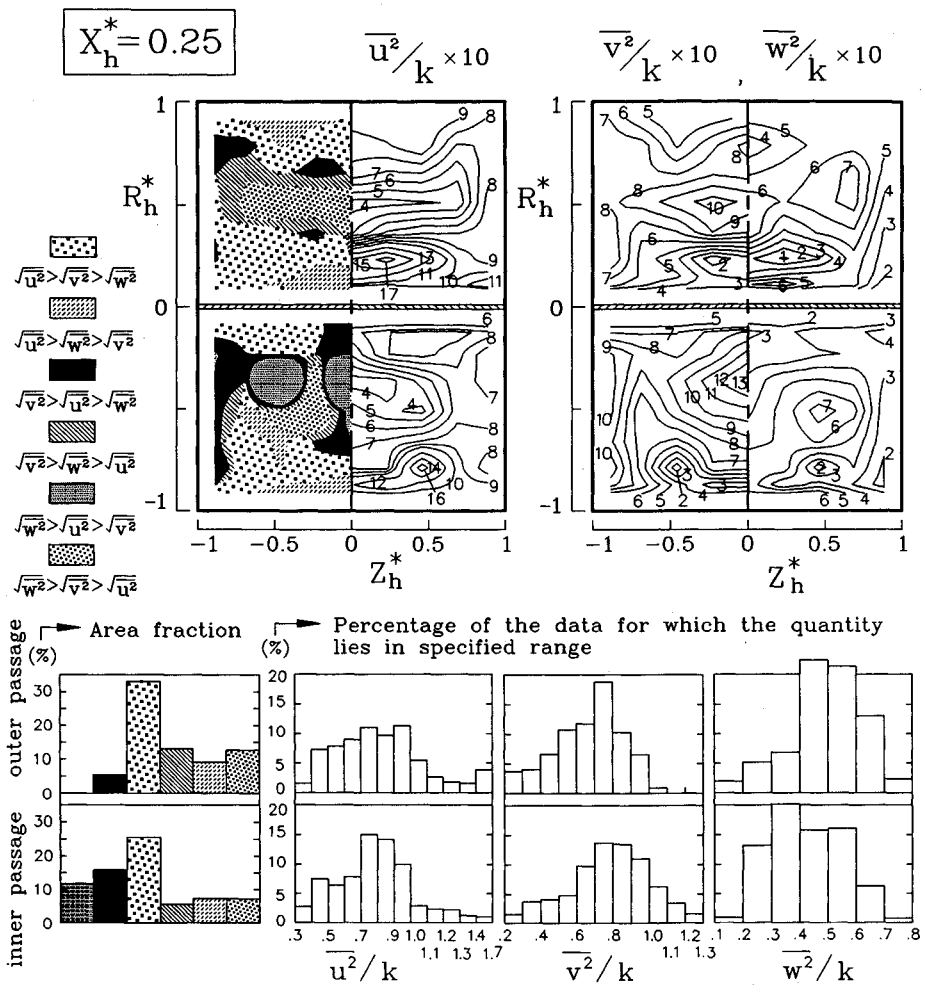

Fig. 11 Distribution of regions of the order of $\sqrt{\overline{u^2}}$, $\sqrt{\overline{v^2}}$, and $\sqrt{\overline{w^2}}$, as well as contour maps and distributions of $\overline{u^2}/k$, $\overline{v^2}/k$, and $\overline{w^2}/k$ at $X_h^* = 0.25$ for one-vane case.

examining the basic assumptions that are integral in the turbulence modeling of the investigated curved flow.

Vorticity

The streamwise mean vorticity, $\Omega = \partial W/\partial R_h - \partial V/\partial Z_h$, is a direct manifestation of the secondary flow.[28] Figure 9 depicts Ω distributions for both one-vane and no-vane cases. The negative vorticity contours are mainly distributed near the side walls, indicating the existence of the counter-rotating main secondary flow vortices; moreover, the positive vorticity contours prevailing near the inner wall at $X_h^* = 0.25$ reveal the presence of an additional pair of secondary flow vortices. Figure 10 shows the variation of Ω_{max} with the streamwise distance. The comparison of Ω_{max} between the two present cases reveals that a stronger main secondary flow vortex is developed within the curved duct with a guide vane than without a guide vane ($9.6U_{ref}/D_h$ as opposed to $6.2U_{ref}/D_h$ at $\theta_h = 60$ deg). This essential character is consistent with the previous discussion of the secondary mean velocity.

Based on the streamwise vorticity transport equation, the difference between the radial and spanwise normal stresses, $\overline{v^2} - \overline{w^2}$, is one of the causes for generation of secondary flow of the second kind,[29,30] and is plotted in Fig. 8 in terms of contours for the one-vane case. It can be seen that the $\overline{v^2} - \overline{w^2}$ contours concentrate near the side walls and inner wall, and the value of $(\overline{v^2} - \overline{w^2})/U_{ref}^2$ is almost zero around the central part of the curved duct. Moreover, the anisotropy between $\overline{v^2}$ and $\overline{w^2}$ near the inner wall is enhanced by the reversed flow. These trends parallel those observed from Ω contours, although $(\overline{v^2} - \overline{w^2})/U_{ref}^2$ is two orders of magnitude smaller than $\Omega D_h/U_{ref}$. It is interesting to note that $\Omega D_h/U_{ref}$ and $(\overline{v^2} - \overline{w^2})/U_{ref}^2$ of the present work are about one order of magnitude larger than those obtained by Yokosawa et al.[29] in the smooth and rough square duct using a hot-wire anemometer, but are of the same order as those reported by Liou et al.[30] in a channel with a rib-disturbed wall using LDV.

Flow Distribution near the Dump Plane

Flow measurements at the dump plane can serve as inlet information for computational simulations of combustor flowfields. Due to blockage of the flange that mounts the inlet duct on the combustor, it is difficult to measure the velocity at the dump plane. The profiles of the longitudinal mean velocity at the $X_h^{**} = 1.11$ station, located at a stage of $0.0875D_h$ above the dump plane along the symmetric plane for both one-vane and no-vane cases, are shown in Fig. 12. The reversed flow at the inner wall enhances higher turbulence intensity at the proximity of the inner wall for the no-vane case. The presence of the guide vane makes the longitudinal mean velocity distribution across the inner passage of the curved duct more uniform, and hence, eliminates the flow reversal near the inner wall at the $X_h^{**} = 1.11$ station, even though the no-slip condition at the guide vane produces a velocity deficit around the guide vane. It should be pointed out that the flow distribution near the dump plane is obviously neither uniform nor similar to one-seventh-power law, which was often assumed by early researchers in modeling combustor flow.[31,32]

The radial mean velocity distributions at $X_h^{**} = 0.63$ and 1.1 (at a stage of 0.5 and $0.1D_h$ above the dump plane, re-

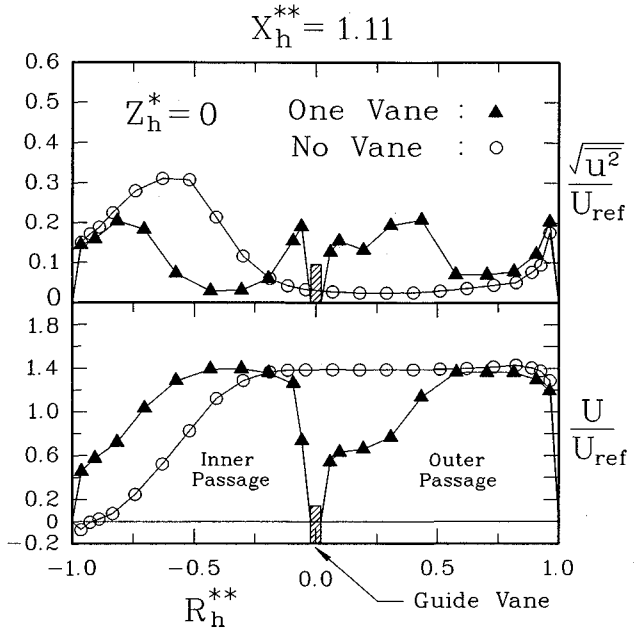

Fig. 12 Longitudinal mean velocity distributions along $Z_h^* = 0$ at $X_h^{**} = 1.11$ station.

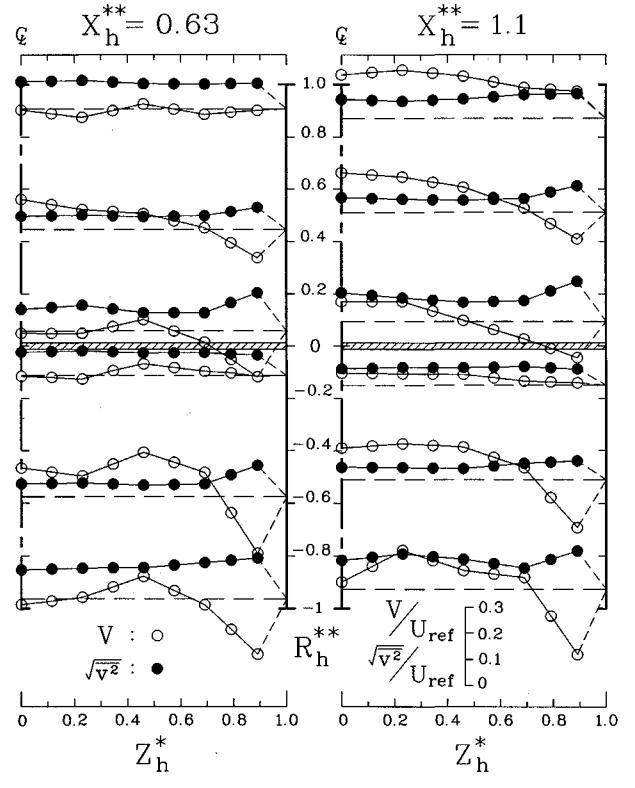

Fig. 13 Distributions of radial mean velocity and turbulence intensity at $X_h^{**} = 0.63$ and $X_h^{**} = 1.1$ for one-vane case.

spectively) are shown in Fig. 13 for the one-vane case. At $X_h^{**} = 0.63$, the secondary flow starts to break down into a system of three pairs of secondary vortices. Apart from the main secondary flow vortices, there are now two pairs of additional secondary flow vortices: one is set up near the central outer wall due to the instability induced by the imbalance between the rapidly decreasing centrifugal force and the inward pressure force; the other prevails near the central inner wall owing to the relatively sluggish fluid element in the reversed flow. As the flow moves to $X_h^{**} = 1.1$, the six-vortex structure decays to a single pair of counter-rotating vortices as a result of the effects of sudden downstream expansion and impingement of the flow inside the combustor. This evolution of the vortex structure can be observed in the lower and upper ducts of a one-vane case and in the duct of a no-vane case in addition to what has been found experimentally by Liou and Liu[9] for the developing turbulent flow in a 90-deg square duct without a downstream combustor and by Cheng et al.[33] for the fully developed laminar flow in 180-deg rectangular channels using flow visualization. The radial turbulence intensity is higher at those regions where higher gradients of the radial mean velocity occur and the maximum radial turbulence intensity is found to be of $0.15U_{ref}$ at the inner wall of $X_h^{**} = 0.63$.

Influence of a Guide Vane

A consequence of introducing a guide vane into the curved duct is a significant reduction of the velocity differences between the inner and outer walls and, hence, a more uniform distribution of the velocity across the inner passage of the curved duct, as shown in Fig. 12. Based on the previous discussion, the main secondary flow vortex is stronger for the one-vane case, which means a stronger cross-stream convection of high velocity fluid and, in turn, a reduction in the size of the reversed flow region. This essential feature corresponds to the two-dimensional computational presentation of Kotb et al.,[21] which states that the size of the recirculating region decreased with the increase in aspect ratio. It can also be observed that the maximum turbulence levels decrease with the addition of a guide vane (see Fig. 10). Moreover, the comparison shows that a lower degree of anisotropy is attained near the inner and outer walls of the one-vane case than at the corresponding walls of the no-vane case. The stronger secondary flow vortices and the more uniform velocity profile in the inner passage can enhance the mixing and impinging effects on the air-fuel mixture recirculated upstream into the dome region of the combustor.[34] Therefore, it is conceivable that the inlet curved duct with a guide vane is beneficial to the successful performance of the combustor.

Summary and Conclusions

The main and secondary flowfields in a 60-deg curved inlet duct with and without a guide vane upstream of a side-dump combustor have been characterized using laser-Doppler velocimetry. The main flow is found to separate at $X_h^* \simeq 0.05$ and $\theta_h \simeq 57$ deg, respectively, along the central inner wall of the duct with and without a guide vane. As the flow proceeds through the bend and its immediately downstream tangent ($X_h^* = 0.25$), the maximum turbulence level increases with increasing streamwise distance while the number of vortex pairs increases from one to two. Further downstream of the bend, the secondary flow structure evolves even more drastically, with vortex pairs of two, three, and one occurring at $X_h^* = 0.25$, $X_h^{**} = 0.63$, and $X_h^{**} = 1.1$, respectively. Three significant changes occur through insertion of the guide vane. The first is suppression of the region of flow reversal; the area of the reversed flow region is reduced to 25% of the original size observed for the case without a guide vane. The reversed flow near the dump plane will lead to a downstream shift of the impingement of two side-inlet jets in the combustor and subsequently affect the size of the flameholding recirculation flow inside the combustor. The second event is that the turbulence levels are lowered and more isotropic. The last is the appearance of a more uniform velocity distribution across the inner passage of the curved duct and the stronger main secondary flow vortex. This enhances the mixing and impinging effects on the air-fuel mixture recirculated upstream into the dome region of the combustor, and has a beneficial effect on the successful performance of the combustor. The present measured three-dimensional flow, e.g., the distributions of structure parameters and streamwise mean velocity, should provide a useful data base to guide and test

theoretical developments for modeling the developing turbulent flow in curved ducts. Moreover, the mean and turbulence data near the dump plane are provided to serve as inlet boundary conditions for more realistic numerical modeling of combustor flows.

Acknowledgment

Support for this work was partially provided by the National Science Council of the Republic of China under Contract NSC-82-0424-E007-034.

References

[1]Ward-Smith, A. J., *Internal Fluid Flow: The Fluid Dynamics of Flow in Pipes and Ducts*, Oxford Univ. Press, Oxford, England, UK, 1980.

[2]Eustice, J., "Experiments on Stream-Line Motion in Curved Pipes," *Proceedings of the Royal Society of London, Series A.*, Vol. 85, 1911, pp. 119–131.

[3]Austin, L. R., and Seader, J. D., "Entry Region for Steady Viscous Flow in Coiled Circular Pipes," *AIChE Journal*, Vol. 20, No. 4, 1974, pp. 820–822.

[4]Agrawal, Y., Talbot, L., and Gong, K., "Laser Anemometer Study of Flow Development in Curved Circular Pipes," *Journal of Fluid Mechanics*, Vol. 85, 1978, pp. 497–518.

[5]Humphrey, J. A. C., Taylor, A. M. K. P., and Whitelaw, J. H., "Laminar Flow in a Square Duct of Strong Curvature," *Journal of Fluid Mechanics*, Vol. 83, Pt. 3, 1977, pp. 509–527.

[6]Humphrey, J. A. C., Whitelaw, J. H., and Yee, G., "Turbulent Flow in a Square Duct with Strong Curvature," *Journal of Fluid Mechanics*, Vol. 103, 1981, pp. 443–463.

[7]Taylor, A. M. K. P., Whitelaw, J. H., and Yianneskis, M., "Curved Ducts with Strong Secondary Motion: Velocity Measurements of Developing Laminar and Turbulent Flow," *Journal of Fluids Engineering*, Vol. 104, Sept. 1982, pp. 350–359.

[8]Holt, M., Flores, J., and Turi, P. J., "Measurements of Air Flow in a Curved Pipe Using Laser-Doppler Velocimetry," *1st International Symposium on Application of LDA to Fluid Mechanics* (Lisbon, Portugal), 1982, pp. 1–5.

[9]Liou, T. M., and Liu, C. H., "An Investigation of Pressure Loss and Mean Velocity Field in a Curved Square Duct with Different Reynolds Numbers," *Journal of the Chinese Society of Mechanical Engineers*, Vol. 7, No. 4, 1986, pp. 243–251.

[10]Liou, T. M., and Wu, S. M., "The Effect of Aspect Ratio on the Air Flow in Curved 90° Ducts with Uniform Inlet Condition," *Journal of the Chinese Institute of Engineers*, Vol. 10, No. 2, 1987, pp. 147–156.

[11]Pratap, V. S., and Spalding, D. B., "Numerical Computation of the Flow in Curved Ducts," *Aeronautical Quarterly*, Vol. 26, Aug. 1975, pp. 219–228.

[12]Iacovides, H., Launder, B. E., Loizou, P. A., and Zhao, H. H., "Turbulent Boundary-Layer Development Around a Square-Sectioned U-Bend: Measurements and Computation," *Journal of Fluids Engineering*, Vol. 112, Dec. 1990, pp. 409–415.

[13]Govindan, T. R., Briley, W. R., and McDonald, H. "General Three-Dimensional Viscous Primary/Secondary Flow Analysis," *AIAA Journal*, Vol. 29, No. 3, 1991, pp. 361–370.

[14]Dong, Z. F., and Ebadian, M. A., "Numerical Analysis of Laminar Flow in Curved Elliptic Ducts," *Journal of Fluids Engineering*, Vol. 113, Dec. 1991, pp. 555–562.

[15]Ghia, K. N., Chia, U., and Shin, C. T., "Study of Fully Developed Incompressible Flow in Curved Ducts, Using a Multi-Grid Technique," *Journal of Fluids Engineering*, Vol. 109, Sept. 1987, pp. 226–236.

[16]Berger, S. A., Talbot, L., and Yao, L. S., "Flow in Curved Pipes," *Annual Review of Fluid Mechanics*, Vol. 15, 1983, pp. 461–512.

[17]Itō, H., "Flow in Curved Pipes," *Japanese Society of Mechanical Engineers International Journal*, Vol. 30, No. 262, 1987, pp. 543–552.

[18]Shah, R. K., and Joshi, S. D., "Convective Heat Transfer in Curved Duct," *Handbook of Single-Phase Convective Heat Transfer*, edited by S. Kakac et al., Wiley-Interscience, New York, 1987.

[19]Madison, R. D., and Parker, J. R., "Pressure Losses in Rectangular Elbows," *Transactions of the American Society of Mechanical Engineers*, Vol. 58, 1936, pp. 167–176.

[20]Itō, H., and Imai, K., "Pressure Losses in Vaned Elbows of a Circular Cross Section," *Transactions of the American Society of Mechanical Engineers, Series D*, Vol. 88, Sept. 1966, pp. 684, 685.

[21]Kotb, N. A. E., Mokhtarzadeh-Dehghan, M. R., and Ward-Smith, A. J., "A Numerical Study of Laminar and Turbulent Flows in a Two-Dimensional Bend with or Without a Guide Vane," *International Journal for Numerical Methods in Engineering*, Vol. 26, 1988, pp. 245–262.

[22]Liou, T. M., and Wu, S. M., "Flowfield in a Dual-Inlet Side-Dump Combustor," *Journal of Propulsion and Power*, Vol. 4, No. 1, 1988, pp. 53–60.

[23]Tsai, M. K., and Liou, T. M., "Study of Flow Induced by Non-uniform Lateral Injection," *Journal of Propulsion and Power*, Vol. 7, No. 5, 1991, pp. 668–677.

[24]Liou, T. M., and Kao, C. F., "Symmetric and Asymmetric Turbulent Flows in a Rectangular Duct with a Pair of Ribs," *Journal of Fluids Engineering*, Vol. 110, Dec. 1988, pp. 373–379.

[25]Liou, T. M., Chang, Y., and Hwang, D. W., "Experimental and Computational Study of Turbulent Flows in a Channel with Two Pairs of Turbulence Promoters in Tandem," *Journal of Fluids Engineering*, Vol. 112, 1990, pp. 302–310.

[26]Chang, S. M., Humphrey, J. A. C., and Modavi, A., "Turbulent Flow in a Strongly Curved U-Bend and Downstream Tangent of Square Cross-Sections," *Physico-Chemical Hydrodynamics*, Vol. 4, No. 3, 1983, pp. 243–269.

[27]Launder, B. E., Reece, G. J., and Rodi, W., "Progress in the Development of a Reynolds-Stress Turbulence Closure," *Journal of Fluid Mechanics*, Vol. 68, Pt. 3, 1975, pp. 537–566.

[28]Perkins, H. J., "The Formation of Streamwise Vorticity in Turbulent Flow," *Journal of Fluid Mechanics*, Vol. 44, Pt. 4, 1970, pp. 721–740.

[29]Yokosawa, H., Fujita, H., Hirota, M., and Iwata, S., "Measurement of Turbulent Flow in a Square Duct with Roughened Walls on Two Opposite Sides," *International Journal Heat and Fluid Flow*, Vol. 10, No. 2, 1989, pp. 125–130.

[30]Liou, T. M., Wu, Y. Y., and Chang, Y., "LDV Measurements of Periodic Fully Developed Main and Secondary Flows in a Channel with Rib-Disturbed Walls," *Journal of Fluids Engineering*, Vol. 115, March 1993, pp. 109–114.

[31]Shahaf, M., Goldman, Y., and Greenberg, J. B., "An Investigation of Impinging Jets in Flow with Sudden Expansion," *Proceedings of the 22nd Israel Annual Conference on Aviation and Astronautics*, 1980, pp. 100–106.

[32]Vanka, S. P., Stull, F. D., and Craig, R. R., "Analytical Characterization of Flow Fields in Side Inlet Dump Combustors," AIAA Paper 83-1399, June 1983.

[33]Cheng, K. C., Nakayama, J., and Akiyama, M., "Effect of Finite and Infinite Aspect Ratios on Flow Patterns in Curved Rectangular Channels," *Flow Visualization*, edited by T. Asanuma, Hemisphere, Washington, DC, 1979, pp. 181–186.

[34]Zetterström, K. A., and Sjöblom, B., "An Experimental Study of Side Dump Ramjet Combustor," *9th International Symposium on Air Breathing Engines*, Beijing, PRC, Sept. 1985, pp. 230–236.